Published in final edited form as:
Neuroscience. 2013 October 10; 250: 773–785. doi:10.1016/j.neuroscience.2013.06.061.

Partial recovery of the damaged rat blood-brain barrier is mediated by adherens junction complexes, extracellular matrix remodeling and macrophage infiltration following focal astrocyte loss

Colin L. Willis[1,*], **Ryan B. Camire**[1], **Stephanie A. Brule**[1], and **David E. Ray**[2]

[1]Department of Biomedical Sciences, College of Osteopathic Medicine, University of New England, 11 Hills Beach Road. Biddeford, ME 04005, USA

[2]MRC Applied Neuroscience Group, School of Biomedical Sciences, Queen's Medical Centre, University of Nottingham NG7 2UH, UK

Abstract

Blood-brain barrier (BBB) dysfunction is a feature of many neurodegenerative disorders. The mechanisms and interactions between astrocytes, extracellular matrix and vascular endothelial cells in regulating the mature BBB are poorly understood. We have previously shown that transitory GFAP-astrocyte loss, induced by systemic administration of 3-chloropropanediol, leads to reversible disruption of tight junction complexes and BBB integrity to a range of markers. However, early restoration of BBB integrity to dextran (10-70 kDa) and fibrinogen was seen in the absence of paracellular tight junction proteins claudin-5 and occludin. In the present study we show that in the GFAP-astrocyte lesioned rat inferior colliculus, paracellular expression of adherens junction proteins (VE-cadherin and β-catenin) was maintained in vascular endothelial cells that lacked paracellular claudin-5 expression and which showed reversible post-translational occludin modification. Claudin-1 expression paralleled the loss and recovery of claudin-5, while claudin -3 or -12 immunoreactivity was not detected. In addition, the extracellular matrix, as visualized by laminin and fibronectin, underwent extensive reversible remodeling and perivascular CD169 macrophages become abundant throughout the lesioned inferior colliculus. At a time that GFAP-astrocytes repopulated the lesion area and tight junction proteins were returned to paracellular domains, the extracellular matrix and leukocyte profiles normalized and resembled profiles seen in control tissue. This study supports the hypothesis that a combination of paracellular adherens junctional proteins, remodeled basement membrane and the presence perivascular leukocytes provide a temporary barrier to limit extravasation of macromolecules and potentially neurotoxic substances into the brain parenchyma until tight junction proteins are restored to paracellular domains.

[*]Correspondence & Present address: Department of Biomedical Sciences, College of Osteopathic Medicine, University of New England, 11 Hills Beach Road. Biddeford, ME 04005, USA cwillis1@une.edu Tel: +1-207-602-2872 .

Keywords

basal lamina; fibronectin; laminin; neurovascular unit; tight junctions; VE-cadherin

Blood-brain barrier (BBB) dysfunction is proposed to play a major role in the pathogenesis of many neurological disorders including multiple sclerosis, stroke, Alzheimer's disease and Parkinson's disease. In health, the BBB is a dynamic structure that is tightly regulated to maintain homoeostasis for neuronal function. The properties of the BBB consist of endothelial cells with tight junctions, astrocyte end-feet surrounding the endothelium, pericytes and basement membrane of the extracellular matrix. Tight junction complexes are composed of transmembrane proteins including members of the claudin multigene family, occludin and junctional adhesion molecule (JAM) proteins and are linked to the actin cytoskeleton through membrane-associated guanylate kinase zonula occludens proteins (ZO-1, -2, -3) (Tsukita et al., 2001; Abbott et al., 2010). Tight junctions can restrict movement of ions inducing high transendothelial electrical resistance (TEER) and polarity in the endothelial cells by forming apical and basal domains. Adherens junctions are largely composed of vascular endothelial (VE)-cadherin and neuronal (N)-cadherin (Bazzoni and Dejana, 2004). These junctional proteins are linked to the actin cytoskeleton via catenin proteins, plakoglobin, α–actinin and vinculin (Weis and Nelson 2006; Harris and Nelson 2010). Adherens junctions are formed in the early stages of developing endothelium, prior to tight junction formation (Bazzoni and Dejana 2004; Lampugnani and Dejana 2007). VE-cadherin deficient mice die mid gestation from major defects in vascular remodeling (Carmeliet et al., 1999). It is unclear whether adherens junctions play a critical role in regulating BBB permeability in the established BBB. However, vessels from β-catenin-null embryos show abnormal lumen morphology, and are frequently hemorrhagic (Cattelino et al., 2003).

The specialized phenotype and function of the BBB is not only dependent on interactions between endothelial cells and cellular components of the BBB microenvironment, but also extracellular matrix proteins and receptors in the endothelial and parenchymal basement membranes of the vascular endothelial cells and glial limitans of astrocytes (Ballabh et al., 2004; Owens et al., 2008; Baeten and Akassoglou 2011). These membranes consist of structural and specialized proteins including laminin isoforms, fibronectin, vitronectin, collagen and heparin sulphate proteoglycans (Tilling et al., 2002; Yurchenco and Patton 2009). Extracellular matrix proteins are potential ligands for integrin and dystroglycan receptors and may regulate cellular processes and signalling between endothelial cells and astrocytes (Milner et al., 2008). The endothelial and parenchymal basement membranes are normally fused and appear as one layer. However, in some pathological states there is disruption of the basement membranes and extracellular matrix and is associated with increased BBB permeability (Rascher et al., 2002, van Horssen et al., 2006). In the developing central nervous system (CNS), macrophages are involved in blood vessel growth (Manoonkitiwongsa et al., 2001; Espinosa-Heidmann et al 2003; Sakurai et al., 2003) and may play a role in maintenance and repair of brain vasculature by production of pro-angiogenic factors and disruption of the extracellular matrix (Fujiyama et al., 2003; Moldovan et al., 2000). Early breakdown of the BBB with extracellular matrix remodeling,

perivascular infiltration and accumulation of leukocytes are features of multiple sclerosis pathology (Kirk et al 2003; Vos et al., 2005; van Horssen et al., 2006). At present, the cellular and basement membrane interactions that regulate BBB integrity are poorly understood.

We have previously shown that astrocytes play a critical role in the expression of tight junction proteins at paracellular domains and in maintaining BBB integrity (Willis et al., 2004a&b). Systemic administration of 3-chloropropanediol induced widespread loss of GFAP immunoreactive astrocytes and endothelial paracellular expression of claudin-5, occludin and ZO-1 in the rat inferior colliculus. Electron microscopy showed swelling of astrocyte cytoplasm and end-feet 6 h after 3-chloropropanediol administration, and by 24 h lesions were well developed with most astrocytes in vulnerable areas severely swollen or necrotic. Loss of GFAP immunoreactivity was maximal by 48 h and was absent from the lesion until astrocytes repopulated the lesion 8-28 days later. Microvessels in the inferior colliculus showed a loss of the normal paracellular localization of tight junction proteins occludin and claudin-5 within 6 h of astrocyte loss. Between 4–8 days, severe down-regulation of tight junction protein expression was observed, which then returned over the same time period as astrocytes repopulated the lesion. The loss of tight junction protein expression correlated with loss of BBB integrity as visualised by vascular leak of a range of markers including gadolium-DTPA (0.5 kDa) (Prior et al., 2004), fluorescently tagged dextran markers (10 and 70 kDa) and fibrinogen (300 kDa) (Willis et al., 2004b). However, leak of dextran (10 and 70 kDa) markers and fibrinogen unexpectedly ceased after 6 days, well before the return of claudin-5 and occludin to appropriate paracellular domains and GFAP immunoreactive astrocytes. This temporal anomaly in BBB integrity has led us to hypothesize that complex interactions in the BBB microenvironment involving adherens junction proteins, extracellular matrix components and macrophage infiltration establish a temporary barrier to limit extravasation of serum proteins and macromolecules in the absence of paracellular tight junction proteins.

This hypothesis was tested in the present study using confocal microscopy and SDS-PAGE/western blotting analysis. Our results show changes in occludin phosphorylation state and paracellular claudin-5 expression at a time when BBB integrity was compromised. These changes in occludin and claudin-5 expression are associated with increased expression and maintenance of paracellular adherens junction proteins VE-cadherin and β-catenin, together with increased laminin and fibronectin expression, a remodeled basement membrane cyto-architecture and marked infiltration of CD169 expressing macrophages into the lesioned area. Our results suggest that a coordinated response in components of the BBB microenvironment restores a degree of vascular integrity limiting extravasation of macromolecules and potentially neurotoxic substances into the parenchyma until tight junction proteins are restored to paracellular domains. The results provide new and important evidence of the brain's dynamic ability to rapidly limit vascular leaks at the BBB, that occur during pathological conditions such as stroke, traumatic brain injury and auto-immune diseases such as multiple sclerosis and neuromyelitis optica (Barnett et al., 2012).

EXPERIMENTAL PROCEDURES

Animals and Dosing

Male Fisher F344 rats (180-220 g; Harlan Indianapolis, IN, USA) were group housed and maintained on a 12:12 h day/night light cycle with food and water provided ad libitum. The rats were given a single i.p. dose of 140 mg/kg (S)-(+)-3-chloro-1,2-propanediol, ((3-chloropropanediol, S-α-chlorohydrin) Sigma-Aldrich Inc., St Louis, MO, USA) in sterile saline (1 ml/kg) under light isoflurane anesthesia. The animals were allowed to recover, monitored daily for signs of ataxia and then killed up to 28 days after dosing. Following 3-chloropropanediol (140 mg/kg i.p.) administration, rats developed a mild truncal ataxia over 48-72 h, with slight weight loss (5-10% body weight). After eight days they had regained weight and behaved normally. Vehicle injected animals were used for control inferior colliculus tissue studies. Four to six animals were used in each group. All procedures and treatments with animals were carried out in accordance with the UK Animals (Scientific Procedures) Act 1986 and Home Office guidelines and approved by the University of New England Institutional Animal Care and Use Committee, and abide by National Institutes of Health guidelines. All efforts were made to minimize the number of animals used and their suffering.

Tissue Preparation

For confocal microscopy and western blot analysis, animals were killed by an over-dose of isoflurane anesthetic followed by decapitation. Brains were rapidly removed and the hind brain or inferior colliculus dissected and snap-frozen in dry ice-cooled isopentane at −40°C and stored at −80°C. For electron microscopy rats were transcardially perfused at a pressure of 120 mm Hg with 0.9% saline for 1 min and then with fixative of 2% paraformaldehyde, 2% glutaraldehyde in 0.1 M sodium cacodylate buffer, pH 7.2 for 12 min. Brains were post fixed for 24 h at 4°C.

Confocal immunofluorescence

Cryostat sections (30 μm) of the inferior colliculus (+0.4 to +0.6 mm from the interaural line) (Paxinos and Wilson 1998) were cut and mounted on gelatin-coated glass slides and stored at −80°C until required. Sections containing the inferior colliculus and cerebellar cortex were air-dried and fixed in 100% ethanol for 10 min. Sections were washed in PBS, then in buffer (1% bovine serum albumin (BSA)/0.2% Tween-20 in PBS) and incubated in normal goat serum (2 mg/ml; Dako A/S, Glostrup, Denmark) in buffer for 30 min. Indirect immunofluorescence was performed using the following antibodies and dilutions: a) mouse antibodies; β-catenin (0.3 μg/ml; BD Transduction Labs, San Jose, CA, USA), CD163 (ED2) (5.0 μg/ml; Serotec, Oxford, UK), CD169 (ED3) (10.0 μg/ml; Serotec), platelet endothelial cell adhesion molecule-1 (PECAM-1/CD31) (0.25 μg/ml; Serotec), glial fibrillary acidic protein (GFAP) (0.8 μg/ml; Sigma-Aldrich Inc., st Louis, MO, USA); b) rabbit antibodies; VE-cadherin (2.0 μg/ml; Enzo Alexis, Plymouth Meeting, PA, USA), claudin-1,-3,-12, occludin (2.5 μg/ml; Invitrogen, Camarillo, CA, USA), laminin (2.0 μg/ml Dako), fibronectin (0.5 μg/ml Sigma-Aldrich). For double label immunofluorescence, polyclonal antibodies were co-incubated with monoclonal antibody to PECAM-1 or β-catenin. Primary antibodies were diluted in buffer and incubated on sections for 2 h.

Sections were then washed in buffer and incubated in purified goat anti-mouse IgG and goat anti-rabbit IgG secondary antibodies conjugated to either Alexa-Fluor-488 or Alexa-Fluor-568 (4 μg/ml; Life Technologies, Carlsbad, CA, USA) for 1 h in the dark. Finally, sections were washed in buffer then PBS and mounted in ProLong Gold antifade (Life Technologies). Isotype-matched normal mouse serum or normal rabbit serum were used as negative reagent controls. All incubations were carried out at room temperature. Sections were assessed for changes in tight- and adherens junctional protein expression, macrophage infiltration and laminin and fibronectin profiles over the course of the study in the inferior colliculus and the neighboring non-vulnerable cerebellar cortex, which was used as an internal control.

Sections were examined using a Leica TCS SP5 laser scanning confocal microscope (Leica, Buffalo Grove, IL, USA) with an argon-krypton laser and three channel scan head. Scans were made sequentially through the 30 μm sections and maximum projection images or a confocal slice obtained which were exported and viewed using Paint Shop Pro 7.0 (Jasc Software, Inc. Eden Prairie, MN, USA) and uniformly adjusted to optimize brightness and contrast.

Electron Microscopy

Sections 500 μm thick were cut in this buffer on a Leica VT1000S vibrating blade microtome (Leica). Selected areas were dissected, secondary-fixed in 1% osmium tetraoxide in cacodylate buffer for 3 h, dehydrated through an ethanol-propylene oxide series, and embedded in araldite. Semi-thin sections were stained with toluidine blue; thin sections with saturated uranyl acetate in ethanol and lead citrate (Venable and Coggeshall, 1965).

SDS-PAGE and western blot analysis

The inferior colliculus was homogenized using a hand held Teflon homogenizer in ice cold CelLytic buffer (Sigma-Aldrich) containing protease inhibitor cocktail (Sigma-Aldrich) and phosphatase inhibitor cocktail 2&3 (Sigma-Aldrich). The homogenate was cleared by centrifugation (10,000g, 10 min, 4°C). Protein concentration of each sample was determined using the bicinchoninic acid protein assay (Pierce Biotechnology, Rockford, IL, USA) and used for western blot analysis.

Tissue homogenates were separated on SDS–polyacrylamide gels (10% Bis-Tris Criterion XT precast gels; Bio-Rad, Hercules, CA, USA). Separated proteins were transferred to polyvinylidene difluoride membranes (Immobilon PVDF, 0.45 μm, Millipore, Billerica, MA, USA). Non-specific binding was blocked with Aquablock (Eastcoast Biologics Inc, North Berwick, ME, USA) for 60 min at room temperature. PVDF membranes were incubated overnight at 4°C with rabbit antibodies to occludin (2.5 μg/ml; Invitrogen), VE-cadherin (2.0 μg/ml; Enzo Alexis), fibronectin (0.5 μg/ml; Sigma-Aldrich), GAPDH (0.1 μg/ml Santa Cruz Biotechnology, Inc. San Francisco, CA, USA) diluted in Aquablock.

PVDF membranes were washed with Tris-Tween buffered saline (TTBS) (30 mM Tris, 150 mM NaCl and 0.5% (vol/vol) Tween 20 at pH 7.4) and incubated with secondary antibody, goat anti-rabbit conjugated to IR Dye 680 (0.1 μg/ml) (LI-COR, Lincoln, NE, USA) in Aquablock for 120 min at room temperature. PVDF membranes were washed in TTBS and

PBS. Protein bands were visualized by infrared laser scanning using the Odyssey Infrared Imaging system (LI-COR). Molecular weights of the protein bands were calculated using Odyssey software and were quantified and corrected for background using ImageJ densitometric software (NIH, Bethesda, MD, USA). Protein levels were normalized to expression of GAPDH, which served as a loading control.

Statistical analysis

Western blot densitometry data are reported as means ± s.e.m. from 3-5 separate experiments in each group. Statistical significance between treatment groups and control values was determined using Student's *t*-test analysis.

RESULTS

Occludin expression and post-translational modification induced by transitory astrocyte loss in the inferior colliculus

The PVDF membranes probed for occludin revealed many bands. These bands have previously been described, as representing monomer, dimer, and oligomer forms of occludin (McCaffrey et al, 2009). In this study, we have studied changes in the 51 and 57 kDa bands. These bands are indicative of phosphorylated and non-phosphorylated states of occludin (Antonetti et al., 1999; Huber et al., 2002). In control tissue a prominent band was seen at 57 kDa with minimal expression of the 51 kDa band (Fig. 1). Following 3-chloropropanediol administration there was a slight decrease (75% of control) in expression of the 57 kDa band by 1 day. However, by 2 days there was a marked increase in expression of both the 51 kDa (127%) and 57 kDa (150%) bands compared to control levels. By 3 days, and peaking at 4 days, there was a significant increase in expression of both 51 kDa (220%, $p<0.01$) and 57 kDa (223%, $p<0.05$) bands. By 6 days, expression of the 51 kDa ($p<0.01$) and 57 kDa ($p<0.01$) bands were significantly increased compared to the control levels, but were beginning to decrease and continued to decrease at 8 days with expression of 51 kDa band 103% of control and 57 kDa band 117% of control (Fig. 1).

Changes in VE-cadherin morphology and expression induced by transitory astrocyte loss in the inferior colliculus

Sections containing the inferior colliculus were double labeled for VE-cadherin and PECAM-1. In control inferior colliculus tissue, VE-cadherin immunoreactivity demonstrated continuous, sharply defined pattern of single lines marking the paracellular margins of adjacent endothelial cells as visualized by PECAM-1 immunoreactivity (Fig. 2A asterisk). In addition, regions of the PECAM-1 immunoreactive endothelial cells showed punctuate VE-cadherin immunoreactivity (Fig. 2A arrows). This pattern of VE-cadherin immunoreactivity was also seen in non-vulnerable regions such as the cortex. Three days after 3-chloropropanediol administration, at a time when we have previously described a marked reduction of claudin-5 and occludin expression at paracellular domains (Willis et al., 2004b), VE-cadherin immunoreactivity was still present as sharply defined staining and that appeared to be increased when compared to control tissue (Fig. 2B asterisk). Punctuate staining (Fig. 2B arrows) was still seen in some vessels. By 4 days, there were extended regions of sharply defined VE-cadherin immunoreactivity (*) compared to non-dosed

inferior colliculus tissue (Fig. 2C asterisk). Eight days after dosing, some regions of sharply defined VE-cadherin immunoreactivity (*) appeared together with punctuate staining (Fig. 2D arrows). By 14-28 days, the sharply defined paracellular VE-cadherin immunoreactivity was present together with punctuate staining and resembled the VE-cadherin profile seen in control inferior colliculus tissue (Fig. 2E&F). VE-cadherin expression in adjacent non-vulnerable cortical regions did not change over the 28 day study period (data not shown).

Western blot analysis was performed on the inferior colliculus and probed for VE-cadherin (Fig. 2G). In control tissue, low levels of VE-cadherin expression was seen at 126 and 184 kDa with high levels of expression at 43 kDa. One day after 3-chloropropanediol administration there was a slight increase in expression of both the 126 kDa ($p<0.05$) and 184 kDa ($p<0.05$) bands of about 20-30% compared to control levels. By 2 days post administration there was a significant increase in expression of both the 126 kDa (228%, $p<0.05$) and 184 kDa (283%, $p<0.01$) bands. VE-cadherin expression peaked at 3-4 days and both the 126 kDa ($p<0.001$) and 184 kDa ($p<0.01$) bands showed between 300-350% increased expression compared to control levels (Fig. 2G). After 4 days, expression of VE-cadherin 126 kDa and 184 kDa bands rapidly decreased so that by 6-8 days levels of 126 and 184 kDa expression were 60-80% of control values (Fig. 2G). Levels of expression of a 43 kDa band showed increased expression ($p<0.05$) compared to control levels at days 3-4 (Fig. 2G).

Comparison between β-catenin and claudin-5 immunoreactivity following transitory astrocyte loss

To study the relationship between adherens and tight junction protein expression following 3-chloropropanediol induced astrocyte loss, sections were double labeled for β-catenin and claudin-5. In non-dosed inferior colliculus tissue, β-catenin immunoreactivity showed the same pattern of expression as VE-cadherin, appearing as a continuous sharply defined pattern of single lines marking the margins of adjacent endothelial cells (Fig. 3A asterisk). Punctate β-catenin staining was not present at this time point. Claudin-5 immunoreactivity (Fig. 3A) mirrored that seen for β-catenin and appeared as a continuous, sharply defined pattern as previously described (Willis et al., 2004b). However, 3 days after 3-chloropropanediol administration there was a marked divergence in β-catenin and claudin-5 immunoreactivity. Paracellular β-catenin immunoreactivity appeared more robust compared to non-dosed inferior colliculus tissue, as was seen for VE-cadherin expression (Fig. 2B), while the claudin-5 immunoreactivity was greatly reduced. The sharply defined paracellular claudin-5 immunoreactivity was disrupted, with regions of diffuse immunoreactivity in the endothelial cells (Fig 3B, dots). By 4 days, β-catenin paracellular immunoreactivity was present in many areas and was comparable to control non-dosed tissue (Fig. 3C asterisk). In contrast, both the sharply defined paracellular immunoreactivity and most of the diffuse cytoplasmic claudin-5 immunoreactivity was lost within PECAM-1 immunoreactive vessels (Fig 3C). Restoration of claudin-5 immunoreactivity started 8 days after dosing and appeared as faint diffuse expression while β-catenin immunoreactivity was maintained at paracellular domains (Fig. 3D asterisk) together with regions of punctuate staining (Fig. 3D arrows). By 14-28 days, the pattern of β-catenin immunoreactivity was comparable to that seen in control non-dosed tissue (Fig. 3E asterisk). Over the same period, claudin-5

immunoreactivity was restored to sharply defined paracellular domains with diffuse cytoplasmic immunoreactivity (Fig. 3F asterisk). This pattern of claudin-5 immunoreactivity mirrored β-catenin expression. Both claudin-5 and β-catenin immunoreactivity at 28 days resembled that seen in control inferior colliculus. Non-vulnerable cerebral cortex tissue showed no change in β-catenin and claudin-5 expression over the 28 day period (data not shown).

Claudin-1, -3, -12 immunoreactivity in the normal and astrocyte-lesioned inferior colliculus

To determine whether following loss of claudin-5 expression there was a compensatory response in the expression of other claudin proteins, sections were immunolabeled for claudin 1, 3 and 12. Temporal changes in claudin-1 expression followed those seen for claudin-5 (data not shown). Claudin-3 or 12 expression was not seen in the rat inferior colliculus over the 28 day experimental period (data not shown).

Modified laminin and fibronectin immunoreactivity and expression with extracellular matrix remodeling

In control inferior colliculus tissue, laminin and fibronectin immunoreactivity was seen in close association with the vasculature and not present in the parenchyma (Fig. 4A&G). At the ultra-structural level, the basement membrane was seen as one fused layer in close association with the underlying endothelial cell (Fig. 4B asterisk). Following 3-chloropropanediol administration there were marked changes in the pattern of laminin and fibronectin expression in the inferior colliculus as the lesion developed. First signs of perturbation in laminin immunoreactivity were observed after 2 days, at a time when GFAP immunoreactive astrocytes were markedly reduced in the inferior colliculus. At this time laminin immunoreactivity increased and became thickened around vascular endothelial cells. In surrounding brain areas that maintained GFAP astrocytes, no change in laminin immunoreactivity was seen (data not shown). At 3-4 days, in the lesioned inferior colliculus laminin and fibronectin deposition and remodeling could be seen (Fig. 4C&H). The smooth laminin and fibronectin profiles were lost and appeared more irregular. Some laminin and fibronectin immunoreactivity was also seen in the parenchyma that did not appear to be associated with the vasculature (Fig. 4C&H arrows). Outside the 3-chloropropanediol-induced lesioned area, the laminin and fibronectin profiles remained unchanged. Between 6-14 days after dosing, extensive laminin rearrangement continued. The laminin profile was highly irregular and laminin immunoreactivity was present throughout the parenchyma of the inferior colliculus (Fig. 4D). Electron microscopy showed that after 8 days there was remodeling of the basement membrane, that had changed from a single fused layer (Fig. 4B) to several non-fused layers of basement membrane surrounding the vascular endothelium (Fig. 4E asterisk). Between these basement membrane layers there was deposition of other extracellular matrix components (Fig 4E diamond). By 28 days, the laminin profile resembled that seen in control non-dosed inferior colliculus tissue (Fig. 4F) appearing as smooth profiles around the underlying endothelial cells. Laminin immunoreactivity was largely absent from the brain parenchyma. Expression of laminin or fibronectin in the adjacent non-vulnerable cerebral cortex, that was used an internal control, did not change over the 28 day period (data not shown).

Western blot analysis of fibronectin expression paralleled the changes reported from tissues sections. In control non-dosed tissue, fibronectin was seen as a single 225 kDa band. Levels of fibronectin expression started to increase 1 day after 3-chloropropanediol administration and continued to increase reaching a peak at 3 days ($p<0.01$). By 8 days, levels of fibronectin expression had decreased and were comparable to those seen in control tissue.

CD169-immunoreactive macrophage and leukocyte infiltration

In undosed animals, a few CD169 immunoreactive macrophages were present in the inferior colliculus (Fig. 5A) or cortical areas. These CD169 macrophages were co-localized with laminin immunoreactive basement membranes. The macrophages generally appeared as long cells with fine processes along the vasculature (Fig. 5A arrows). At the ultra-structure level, no leukocytes were seen (Fig. 5B). 2-3 days following 3-chloropropanediol administration, CD169 immunoreactive macrophages infiltrated the inferior colliculus. These macrophages were seen clustered around the laminin immunoreactive basement membrane (Fig. 5C asterisk), and in the parenchyma (Fig. 5C arrows). Electron microscopy confirmed leukocyte infiltration in the parenchyma and around blood vessels of the lesioned inferior colliculus. In some regions, perivascular macrophages had extended processes to almost completely surround the vascular endothelium (Fig. 5D asterisk). At 4 days, leukocyte infiltration continued with increased numbers of CD169 immunoreactive macrophages present within the lesion. Many of these macrophages still appeared to be associated with the laminin immunoreactive vasculature (Fig. 5E asterisk), but many more were present in the parenchyma of the lesioned inferior colliculus (Fig. 5E, arrows). A similar pattern could also be seen at the ultra-structure level with many different leukocytes present around the vasculature positioned between separated basement membranes (Fig. 5F asterisk) and in the parenchyma (Fig. 5F arrow) of the inferior colliculus. Peak CD169 expression and leukocyte infiltration was seen at 6-8 days with these cells densely packed around the vasculature and in the parenchyma of the inferior colliculus (Fig. 5G&H). Between 14-28 days, the density of CD169 immunoreactive macrophages in the lesion decreased (data not shown). This coincided with repopulation of the lesioned area by GFAP-positive astrocytes and decrease in laminin immunoreactivity. By 28 days, few leukocytes were present in the lesion and the morphology of the tissue began to resemble that seen in control tissue. All of these changes were specific to 3-chloropropanediol lesioned inferior colliculus and no changes in CD169 immunoreactivity or leukocyte infiltration were seen in non-vulnerable cortical areas. Sections from control and lesioned tissue were also labeled for CD163, but no immunoreactivity was seen.

DISCUSSION

This study demonstrates an important difference in the regulation of adherens and tight junction proteins in endothelial cells at the BBB, but also the dynamic nature of the BBB microenvironment in restoring a degree of barrier integrity in a pathological state. We have shown for the first time that following loss of GFAP-immunoreactive astrocytes and paracellular tight junction protein expression in the rat inferior colliculus there was; (i) post-translational occludin modification, ii) continued paracellular morphology and expression of VE-cadherin and β-catenin junctional proteins, (iii) no up-regulation of claudin 1,-3,-12, (iv)

substantial extracellular matrix remodeling and (v) marked leukocyte infiltration, including CD169 immunoreactive macrophages surrounding vascular endothelial cells. These results support our hypothesis that adherens junction proteins, a remodeled basement membrane and infiltration of macrophages provide a temporary barrier at the neurovascular unit to limit extravasation of serum proteins and macromolecules reaching the brain parenchyma until tight junction proteins are restored to paracellular domains.

Systemic 3-chloropropanediol administration induces loss of GFAP-expressing astrocytes in ventrolateral thalamic nuclei, occulomotor and red nuclei, inferior colliculi, vestibular, trigeminal and facial nuclei while in other non-vulnerable regions, such as the cerebral cortex, astrocytes remained intact and were unaffected in terms of tight junction molecules and dextran and fibrinogen leak (Willis et al., 2004a). The mechanism of action and why specific brain areas are vulnerable to the gliotoxin is currently under investigation. 3-Chloropropanediol is metabolized to 3-chlorolactaldehyde, an inhibitor of glyceraldehyde 3-phosphate dehydrogenase (GAPDH) and triose isomerase and so may reflect a regional difference in the dependence on glycolysis.

It has been reported that many astrocytes in the normal brain may not be GFAP immunoreactive and that GFAP-negative astrocytes predominate in gray matter (Levison and Goldman, 1993; Privat et al., 1995). We have previously used a number of techniques to show loss of astrocytes following administration of 3-chloropropanediol. Light and confocal immunohistochemical studies demonstrated a rapid loss of GFAP immunoreactive astrocytes in vulnerable regions. After 6-8 days there was upregulation of GFAP and vimentin expression in astrocytes around the lesion margin, but not in the centre of the lesion (Willis et al., 2004a). Electron microscopy, also showed an absence of astrocyte-like figures within the inferior colliculus, which might have down-regulated their GFAP expression levels (Willis et al., 2004). We cannot exclude the persistence of some perivascular astrocyte endfeet membranes on the microvessels (Cavanagh et al., 1993), but studies have shown astrocytes may need to express GFAP to influence BBB properties. Astrocytes from aged GFAP-deficient mice, showed an impaired BBB (Liedtke et al., 1996), and failed to induce a functional barrier in cultured aortic endothelial cells (Pekny et al., 1998).

Several factors have been identified to regulate BBB permeability including post-translational modification of tight junction proteins. Changes in occludin phosphorylation at both tyrosine and serine/threonine sites have been correlated with changes in BBB permeability (Gonzalez-Mariscal et al., 2008). Western blot analysis has shown two migrating bands (α and β bands) demonstrating occludin post-translational modification (Antonetti et al., 1999). In our present study, two occludin bands were seen at 51 and 57 kDa. There was increased expression of the 57 kDa band at a time when there is loss of paracellular occludin expression and increased BBB permeability (Willis et al., 2004b). At 8 days, there was decreased expression of the 57 kDa band, at a time when GFAP-immunoreactive astrocytes returned to the lesioned area, occludin was seen at paracellular domains and there was decreased BBB permeability. In another study, we have also shown an acute increase in expression of occludin β band as BBB integrity was compromised under 60 min hypoxic (6% O_2) conditions (Willis et al., 2010). In this hypoxia study it was

proposed that there was a rapid change in tight junction phosphorylation state through that action of protein kinase C isozymes. It will be interesting to see if GFAP-astrocyte mediated loss of BBB integrity induces a similar change in protein kinase C isozyme activation and tight junction protein post-translation modification as seen in acute hypoxic induced changes. Together these studies, and others, support the hypothesis that occludin phosphorylation reduces BBB integrity.

In vascular endothelial cells, the major component of adherens junctions is VE-cadherin, a transmembrane protein linked to the cytoskeleton by α-catenin, β-catenin, γ-catenin, plakoglobin and p120 (Dejana et al., 2008; Harris and Nelson 2010). In the present study, confocal microscopy showed that following astrocyte loss, VE-cadherin and β-catenin paracellular immunoreactivity was maintained in contrast to claudin-5 which showed a relatively early (2-3 days) and prolonged loss of immunoreactivity. The loss of paracellular occludin and ZO-1 immunoreactivity has also been reported previously (Willis et al., 2004b). Western blot analysis showed a marked transitory increase in expression of VE-cadherin expression. One day after systemic 3-chloropropanediol administration there was increased expression of VE-cadherin 126 and 184 kDa bands. This coincides with early morphological changes in astrocytes as revealed by electron microscopy and immunofluorescence (Willis et al., 2004b). VE-cadherin expression increased over the 2-4 day period post 3-chloropropanediol administration at a time when GFAP-immunoreactive astrocytes were lost and there was increased expression of post-translation modified 57 kDa occludin band. The expression of β-catenin remained constant over the course of the study. We propose that the difference in the temporal expression of paracellular adherens and tight junction proteins may in part explain the anomaly in our earlier functional data that showed cessation of leak to >10 kDa in the absence of tight junction proteins.

The present study also reveals an important difference in the regulation of adherens junction and tight junction complexes. The loss of GFAP immunoreactive astrocytes results in the loss of paracellular tight junction protein expression, but not paracellular adherens junction protein expression. The mechanisms regulating adherens and tight junction expression are unclear, although many kinases and phosphatases are present with adherens and tight junction proteins at the plasma membrane (Gonzalez-Mariscal et al., 2008; Dejana et al., 2008). Hollande et al., (2003) has shown a difference in the mechanisms regulating tight and adherens junctions. An epithelial cell line treated with progastrin, showed disruption of both tight and adherens junction complexes. However, stimulation of Src kinase activity was essential for the regulation of tight junction proteins while dissociation of adherens junction proteins involved phosphatadylinositol 3-kinase and protein kinase-Cα (Hollande et al., 2003). Vascular endothelial growth factor (VEGF), tumor necrosis factor-α, platelet activating factor and TGF-β1 have been shown to induce tyrosine phosphorylation of VE-cadherin with an increase in vascular permeability (Dejena et al., 2008; Shen et al., 2011). Changes in the astrocytic production of inflammatory cytokines may play a key role in the regulation of BBB integrity in this study.

Claudin-1, -3, -5 and -12 isoforms have been detected in the cerebral microvascular endothelium (Nitta et al., 2003; Wolburg et al., 2003). We found there was a reversible loss of diffuse cytoplasmic claudin-1 immunoreactivity comparable to that previously reported

for claudin-5, and that claudin -3 or -12 immunoreactivity was not seen at any time point in the lesioned inferior colliculus. Therefore, an early return of claudin isoforms does not explain the early cessation of macromolecular leakage.

An essential component of the BBB microenvironment is the extracellular matrix of the basement membranes. Basement membranes located between endothelial cells and astrocytes are well positioned to regulate BBB integrity. Endothelial and glial-parenchymal basement membranes contain laminin isoforms, fibronectin, vitronectin, collagen, and heparin sulphate proteoglycans (Tilling et al., 2002; Yurchenco and Patton 2009). In this study, we probed for laminin and fibronectin to define the basement membranes and have shown extensive remodeling with multiple non-fused basement membranes around the vasculature and parenchyma of the inferior colliculus. At the ultra-structure level, there was evidence of collagen deposition and other extracellular matrix components within these multiple basement membrane layers. The source of the increased laminin expression is unclear and future studies will probe for specific laminin isoforms. At the BBB there are four main laminin isoforms. Laminin isoforms 1 and 2 are found mainly in the astrocytic parenchymal basement membrane and laminin 8 and laminin 10 are present in the endothelial basement membrane (Tilling et al., 2002; Owens et al., 2008). We speculate that the increase in laminin expression seen is from endothelial cells since astrocytes are absent. The remodeling of the extracellular matrix with increased laminin and fibronectin expression and multiple basement membrane layers was seen at a time when tight junction proteins were absent from paracellular domains, but when vascular leak of macromolecules (>10 kDa) had stopped. This supports the hypothesis that the extracellular matrix plays a key role in the formation of a transitory size-selective barrier. The pathological events in our study follow a similar sequence of events to that seen following CNS stab wound injury. Szabo and Kalman (2004) reported that brain vasculature initially showed increased laminin immunoreactivity that subsequently decreased as gliovascular connections were established. Our study demonstrates that the basement membrane is an active component capable of rapid remodeling under pathological conditions and plays a key role, together with adherens junctions, in restoring partial BBB integrity.

The mechanisms regulating glial-endothelial interactions at the BBB are unclear, but may be mediated through integrin receptors. Integrins are transmembrane receptors expressed on astrocytes and endothelial cells (Wu and Reddy 2012). Integrins play an important role in maintaining BBB integrity by forming complexes with cadherin and cell adhesion molecules, forming a physical transmembrane link between the extracellular matrix and the cytoskeleton. Integrins bind cell surface and extracellular matrix components such as fibronectin, vitronectin, collagen and laminin (Milner et al., 2008; Wu and Reddy 2012).

Following GFAP-immunoreactive astrocyte loss and increased BBB permeability, peripheral CD169 immunoreactive macrophages infiltrate the lesion. Initially they are perivascular in location where they may actively contribute to degradation and remodeling of the extracellular matrix. The phagocytic function and perivascular location of these macrophages suggests they play a role in barrier functions sequestering macromolecules leaking across an expanded extracellular matrix. Macrophages have been shown to play a role in BBB reformation after hypothermic brain injury (Koneru et al., 2011) and in studies

using the experimental autoimmune encephalomyelitis model (Ladewig et al., 2009). Therefore, we propose that infiltrating macrophages in the 3-chloropropanediol induced lesion, play a key role in limiting the extent of macromolecule extravasation from the compromised BBB following injury, while integrity of the BBB is restored.

Further, we base this hypothesis on observations from an earlier study of the fenestrated endothelium of the area postrema (Willis et al., 2007). Endothelial cells in the area postrema lack claudin-5 or occludin expression, but do express VE-cadherin. There is also a highly modified extracellular matrix with resident phagocytic perivascular CD163 and CD169 expressing macrophages within non-fused basement membranes (Willis et al., 2007). We hypothesized that this morphological profile imparts size-selective barrier properties since, in the rat, a single intravenous injection of sodium fluorescein (0.3 kDa) rapidly passed through the area postrema and was seen in the surrounding nucleus of the solitary tract, while intravenous administration of 3 kDa dextran was retained within the area postrema and showed a diffuse distribution throughout the area postrema parenchyma. Administration of larger dextrans (10 & 70 kDa) were sequestered by the perivascular CD163 & CD169 immunoreactive macrophages resident within the outer basal lamina surrounding the vascular endothelium and seen not in the parenchyma (Willis et al., 2007). Comparing these results from normal area postrema with those from the pathological response in the lesioned inferior colliculus we see similar morphological modifications. Both the astrocyte lesioned inferior colliculus and the area postrema show modified GFAP astrocyte expression, presence of VE-cadherin and absence of claudin-5 protein expression, modified extracellular matrix profiles and non-fused basement membranes containing phagocytic macrophages. Rapid restoration of limited BBB properties in the injured brain would be critical for minimizing neuronal damage and restoring brain function, since substantial loss of BBB integrity may lead to neuronal damage by exposing the brain to blood borne proteins including potentially neurotoxic albumin (66 kDa) (Hassel et al., 1994).

Conclusion

Our results suggest that the early recovery of vascular integrity to >10 kDa tracers that occurs while occludin shows post-translational modification and prior to the reappearance of paracellular tight junction proteins, is the result of (i) continued paracellular adherens junction protein expression in the absence of tight junction proteins, (ii) a highly remodeled extracellular matrix and (iii) large numbers of perivascular macrophages present within the remodeled extracellular matrix. These observations, together with the morphological parallels drawn with the normal area postrema, lead us to propose that dynamic regulation of the BBB microenvironment rapidly establishes a size-selective barrier that excludes blood components such as serum protein albumin until the vasculature is fully repaired and tight junctional proteins claudin-5, occludin and ZO-1 are restored to paracellular domains. A greater in vivo understanding of the complex interactions between astrocytes, extracellular matrix, vascular endothelial cells and BBB integrity is vital in the development of novel therapeutic targets and drugs. A prominent feature of multiple sclerosis pathology is loss of paracellular tight junction protein expression and BBB integrity, perivascular accumulation of macrophages and lymphocytes and remodeling of the extracellular matrix (Kirk et al., 2003; van Horssen et al., 2005; 2006). In addition, auto-immune mediated astrocyte loss is

reported to be an early event in neuromyelits optica, an inflammatory demyelinating disease of the CNS (Wingerchuk et al., 2007; Barnett et al., 2012). Therefore, the experiments described in this study represent a powerful new paradigm for the understanding of many neurological disorders that show changes in BBB integrity and glial pathology such as stroke, traumatic brain injury, multiple sclerosis and neuromyelitis optica.

Acknowledgments

This work was supported by the American Heart Association SDG2170105 (CLW), a Medical Research Council UK programme grant, and the Office of Research and Scholarship and Center for Excellence in the Neurosciences, University of New England.

REFERENCES

Abbott NJ, Patabendige AA, Dolman DE, Yusof SR, Begley DJ. Structure and function of the blood-brain barrier. Neurobiol Dis. 2010; 37:13–25. [PubMed: 19664713]

Antonetti DA, Barber AJ, Hollinger LA, Wolpert EB, Gardner TW. Vascular endothelial growth factor induces rapid phosphorylation of tight junction proteins occludin and zonula occluden 1. J Biol Chem. 1999; 274:23463–23467. [PubMed: 10438525]

Ballabh P, Braun A, Nedergaard M. The blood-brain barrier: An overview: Structure, regulation and clinical implications. Neurobiol Dis. 2004; 16:1–13. [PubMed: 15207256]

Baeten KM, Akassoglou K. Extracellular matrix and matrix receptors in blood-brain barrier formation and stroke. Develop Neurobiol. 2011; 71:1018–1039.

Barnett MH, Prineas JW, Buckland ME, Parratt JDE, Pollard JD. Massive astrocyte destruction in neuromyelitis optica despite natalizumab therapy. Multiple Sclerosis Journal. 2012; 18:108–112. [PubMed: 21868485]

Bazzoni G, Dejana E. Endothelial cell-to-cell junctions: molecular organization and role in vascular homeostasis. Physiol Rev. 2004; 84:869–901. [PubMed: 15269339]

Cattelino A, Liebner S, Gallini R, Zanetti A, Balconi G, Corsi A, Bianco P, Wolburg H, Moore R, Oreda B, et al. The conditional inactivation of the beta-catenin gene in endothelial cells causes a defective vascular pattern and increased vascular fragility. J Cell Biol. 2003; 162:1111–1122. [PubMed: 12975353]

Carmeliet P, Lampugnani MG, Moons L, Breviario F, Compernolle V, Bono F, Balconi G, Spagnuolo R, Oosthuyse B, Dewerchin M, et al. Targeted deficiency or cytosolic truncation of the VE-cadherin gene in mice impairs VEGF-mediated endothelial survival and angiogenesis. Cell. 1999; 98:147–157. [PubMed: 10428027]

Cavanagh JB, Nolan CC, Seville MP. The neurotoxicity of α-chlorohydrin in rats and mice. I. Evolution of the cellular changes. Neuropathol Appl Neurobiol. 1993; 19:240–252. [PubMed: 8355810]

Dejana E, Orsenigo F, Lampugnani MG. The role of adherens junctions and VE-cadherin in the control of vascular permeability. J Cell Sci. 2008; 121:2115–2122. [PubMed: 18565824]

Espinosa-Heidmann DG, Suner IJ, Hernandez EP, Monroy D, Csaky KG, Cousins SW. Macrophage depletion diminishes lesion size and severity in experimental choroidal neovascularization. Invest Ophthalmol Vis Sci. 2003; 44:3586–3592. [PubMed: 12882811]

Fujiyama S, Amano K, Uehira K, Yoshida M, Nishiwaki Y, Nozawa Y, Jin D, Takai S, Miyazaki M, Egashira K, Imada T, Iwasaka T, Matsubara H. Bone marrow monocyte lineage cells adhere on injured endothelium in a monocyte chemoattractant protein-1-dependent manner and accelerate re-endothelialization as endothelial progenitor cells. Circ Res. 2003; 93:980–989. [PubMed: 14525810]

Gonzalez-Mariscal L, Tapia R, Chamorro D. Crosstalk of tight junction components with signalling pathways. Biochimica et Biophysica Acta. 2008; 1778:729–756. [PubMed: 17950242]

Harris ES, Nelson WJ. VE-cadherin: At the front, center, and sides of endothelial cell organization and function. Curr Opin Cell Biol. 2010; 22:651–658. [PubMed: 20708398]

Hassel B, Iversen EG, Fonnum F. Neurotoxicity of albumin in vivo. Neurosci Letts. 1994; 167:29–32. [PubMed: 7909931]

Hollande F, Lee DJ, Choquet A, Roche S, Baldwin GS. Adherens junctions and tight junctions are regulated via different pathways by progastrin in epithelial cells. J Cell Sci. 2003; 116:1187–1197. [PubMed: 12615962]

Huber JD, Hau VS, Borg L, Campos CR, Egleton RD, Davis TP. Blood-brain barrier tight junctions are altered during a 72-h exposure to λ-carrageenan-induced inflammatory pain. Am J Physiol. 2002; 283:H1531–H1537.

Kirk J, Plumb J, Mirakhur M, McQuaid S. Tight junctional abnormality in multiple sclerosis white matter affects all calibers of vessels and is associated with blood-brain barrier leakage and active demyelination. J Pathol. 2003; 201:319–327. [PubMed: 14517850]

Koneru R, Kobiler D, Lehrer S, Li J, van Rooijen N, Banerjee D, Glod J. Macrophages play a key role in early blood brain barrier reformation after hypothermic brain injury. Neurosci Letts. 2011; 501:148–151. [PubMed: 21782894]

Lampugnani MG, Dejana E. Adherens junctions in endothelial cells regulate vessel maintenance and angiogenesis. Thromb Res. 2007; 120:S1–6. [PubMed: 18023702]

Ladewig G, Jestaedt L, Misselwitz B, Solymosi L, Toyka K, Bendszus M, Stoll G. Spatial diversity of blood–brain barrier alteration and macrophage invasion in experimental autoimmune encephalomyelitis: a comparative MRI study. Exp Neurol. 2009; 220:207–211. [PubMed: 19733560]

Levison, SW.; Goldman, JE. Astrocyte origins. In: Murphy, S., editor. Astrocytes: pharmacology and function. Academic Press; San Diego, CA: 1993. p. 1-22.

Liedtke W, Edelmann W, Bieri PL, Chiu F-C, Cowan NJ, Kucherlapati R, Raine CS. GFAP is necessary for the integrity of CNS white matter architecture and long-term maintenance of myelination. Neuron. 1996; 17:607–615. [PubMed: 8893019]

Manoonkitiwongsa PS, Jackson-Friedman C, McMillan PJ, Schultz RL, Lyden PD. Angiogenesis after stroke is correlated with increased numbers of macrophages: the clean-up hypothesis. J Cereb Blood Flow Metab. 2001; 21:1223–1231. [PubMed: 11598500]

McCaffrey G, Willis CL, Staatz WD, Nametz N, Quigley CA, Hom S, Lochhead JJ, Davis TP. Occludin oligomeric assembly at tight junctions of the blood–brain barrier are altered by hypoxia and reoxygenation. J Neurochem. 2009; 110:58–71. [PubMed: 19457074]

Milner R, Hung S, Wang X, Berg GI, Spatz M, del Zoppo GJ. Responses of endothelial cells and astrocyte matrix-integrin receptors to ischemia mimic those observed in the neurovascular unit. Stroke. 2008; 39:191–197. [PubMed: 18032737]

Moldovan PJ, Goldschmidt-Clermont J, Parker-Thornburg SD, Shapiro PE, Kolattukudy. Contribution of monocytes/macrophages to compensatory neovascularization: the drilling of metalloelastase-positive tunnels in ischemic myocardium. Circ Res. 2000; 87:378–384. [PubMed: 10969035]

Nitta T, Hata M, Gotoh S, Seo Y, Sasaki H, Hashimoto N, Furuse M, Tsukita S. Size-selective loosening of the blood-brain barrier in claudin-5 deficient mice. J Cell Biol. 2003; 161:653–660. [PubMed: 12743111]

Owens T, Bechmann I, Engelhardt B. Perivascular spaces and the two steps to neuroinflammation in mouse models of Alzheimer's disease. J Exp Med. 2008; 204:1999–2008.

Paxinos, G.; Wilson, C. The rat brain in stereotaxic co-ordinates. 4th edit. Academic press; San Diego: 1998.

Pekny M, Stanness KA, Eliasson C, Betsholtz C, Janigro D. Impaired induction of blood-brain barrier properties in aortic endothelial cells by astrocytes from GFAP-deficient mice. Glia. 1998; 22:390–400. [PubMed: 9517571]

Prior MJW, Brown AM, Mavroudis G, Lister T, Ray DE. MRI characterization of a novel rat model of focal astrocyte loss. MAGMA. 2004; 17:125–132. [PubMed: 15592947]

Privat, A.; Gimenez-Ribotta, M.; Ridet, J-L. Morphology of astrocytes. In: Kettenmann, H.; Ranson, BR., editors. Neuroglia. Oxford Press; New York: 1995. p. 3-22.

Rascher G, Fischmann A, Kroger S, Duffner F, Grote EH, Wolburg H. Extracellular matrix and the blood-brain barrier in glioblastoma multiforme: spatial segregation of tenascin and agrin. Acta Neuropathol (Berl). 2002; 104:85–91. [PubMed: 12070669]

Sakurai E, Anand A, Ambati BK, van Rooijen N, Ambati J. Macrophage depletion inhibits experimental choroidal neovascularization. Invest Ophthalmol Vis Sci. 2003; 44:3578–3585. [PubMed: 12882810]

Shen W, Li S, Chung SH, Zhu L, Stayt J, Su T, Courand P-O, Romero IA, Weksler B, Gillies MC. Tyrosine phosphorylation of VE-cadherin and claudin-5 is associated with TGF-β1 permeability of centrally derived vascular endothelium. European J Cell Biol. 2011; 90:323–332. [PubMed: 21168935]

Szabo A, Kalman M. Disappearance of the post-lesional laminin immunopositivity of brain vessels is parallel with the formation of gliovascular junctions and common basal lamina. A double-labelling immunohistochemical study. Neuropath Appl Neurobiol. 2004; 30:169–177.

Tilling T, Engelbertz C, Decker S, Korte D, Huwel S, Galla H-J. Expression and adhesive properties of basement membrane proteins in cerebral capillary endothelial cell cultures. Cell Tissue Res. 2002; 310:19–29. [PubMed: 12242480]

Tsukita S, Furuse M, Itoh M. Multifunctional strands in tight junctions. Nature Rev Mol Cell Biol. 2001; 2:285–293. [PubMed: 11283726]

van Horssen J, Bo L, Vos CMP, Virtanen I, de Vries HE. Basement membrane proteins in multiple sclerosis-associated inflammatory cuffs: potential role in influx and transport of leukocytes. JNEN. 2005; 64:722–729.

van Horssen J, Bo L, Dijkstra CD, de Vries HE. Extensive extracellular matrix depositions in active multiple sclerosis lesions. Neurobiol Dis. 2006; 24:484–491. [PubMed: 17005408]

Venable JH, Coggeshall R. A simplified lead citrate stain for use in electron microscopy. J Cell Biol. 1965; 25:407–408. [PubMed: 14287192]

Vos CM, Geurts JJ, Montagne L, van Haastert ES, Bo L, van der Valk P, Barkhof F, de Vries HE. Blood-brain barrier alterations in both focal and diffuse abnormalities on postmortem MRI in multiple sclerosis. Neurobiol Dis. 2005; 20:953–960. [PubMed: 16039866]

Weis WI, Nelson WJ. Re-solving the cadherin-catenin-actin conundrum. J Biol Chem. 2006; 281:35593–35597. [PubMed: 17005550]

Willis CL, Nolan CC, Reith SN, Lister T, Prior MJW, Guerin CJ, Mavroudis G, Ray DE. Focal astrocyte loss leads to microvascular damage, with subsequent repair of the blood-brain barrier without direct astrocytic contact. Glia. 2004a; 45:325–337. [PubMed: 14966864]

Willis CL, Leach L, Clarke GJ, Nolan CC, Ray DE. Reversible disruption of tight junction complexes in the rat blood-brain barrier, following transitory focal astrocyte loss. Glia. 2004b; 48:1–13. [PubMed: 15326610]

Willis CL, Garwood CJ, Nolan CC, Clarke GJ, Ray DE. A size selective CNS barrier in the rat area postrema formed by perivascular macrophages and the extracellular matrix. Neurosci. 2007; 150:498–509.

Willis CL, Meske DS, Davis TP. Protein kinase C activation modulates reversible increase in cortical blood-brain barrier permeability and tight junction protein expression during hypoxia and posthypoxic reoxygenation. JCBFM. 2010; 30:1847–1859.

Wingerchuk DM, Lennon VA, Lucchinetti CF, Pittock SJ, Weinshenker BG. The spectrum of neuromyelitis optica. Lancet Neurol. 2007; 6:805–815. [PubMed: 17706564]

Wolburg H, Wolburg-Buchholz K, Kraus J, Rascher-Eggstein G, Liebner S, Hamm S, Duffner F, Grote EH, Risau W, Engelhardt B. Localization of claudin-3 in tight junctions of the blood-brain barrier is selectively lost during experimental autoimmune encephalomyelitis and human glioblastoma multiforme. Acta Neuropathol. 2003; 105:586–592. [PubMed: 12734665]

Wu X, Reddy DS. Integrins as receptor targets for neurological disorders. J Pharm Therapeutics. 2012; 134:68–81.

Yurchenco PD, Patton BL. Developmental and pathogenic mechanisms of basement membrane assembly. Curr Pharm Des. 2009; 15:1277–1294. [PubMed: 19355968]

Highlights

- Paracellular VE-cadherin and β-catenin maintained in absence of GFAP-astrocytes.
- Demonstrates different regulation mechanism for adherens and tight junction protein.
- Extracellular matrix remodeling and inflammatory response following astrocyte loss.
- Size-selective temporary barrier formed in the absence of tight junction proteins.
- Represents a new approach to studying BBB integrity loss in demyelinating disorders.

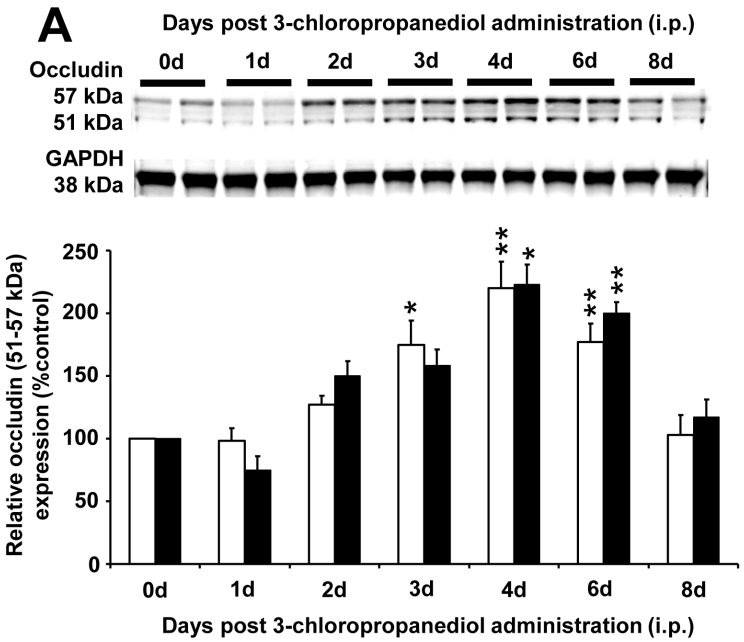

Figure 1.

Western blot analysis showing changes in occludin expression in rat inferior colliculus following 3-chloropropanediol-induced loss of GFAP immunoreactive astrocytes. Occludin expression appeared as two bands at 51 kDa (white bars) and 57 kDa (black bars). Both occludin bands showed increased expression following 3-chloropropanediol administration that peaked at 4 days. By 6-8 days, expression levels of both occludin bands were decreasing, but were still elevated compared to control levels. Protein quantification data was obtained by densitometry and was normalized using glyceraldehyde 3-phosphate dehydrogenase (GAPDH) as loading control. Values are expressed as relative optical density and are represented as mean ± s.e.m. *p<0.05, **p<0.01, compared to the control group. For each column n=4 rats.

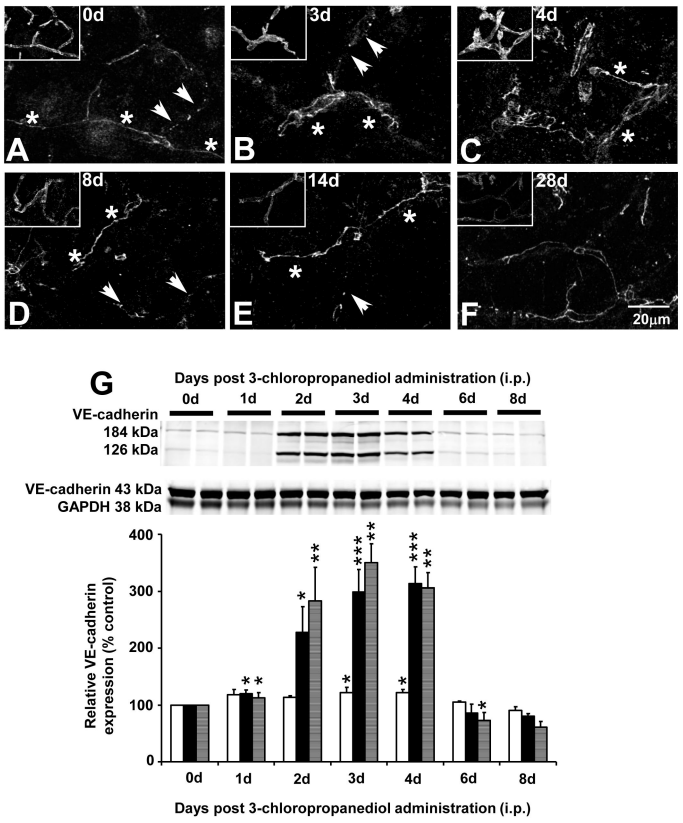

Figure 2.

Confocal micrographs and western blot analysis showing changes in VE-cadherin morphology and expression following 3-chloropropanediol-induced changes in the inferior colliculus. Tissue sections were double labeled for VE-cadherin and PECAM-1. (A) VE-cadherin immunoreactivity (main images) in control (0 days) inferior colliculus demonstrated both sharply defined staining (*) and punctuate staining (arrow) along the margins of PECAM-1 immunopositive brain endothelial cells (insets). (B) At 3 days, a similar picture of VE-cadherin immunoreactivity was seen with both sharply defined staining (*) and punctate staining (arrow), (C) At 4 days, VE-cadherin immunoreactivity appeared to be increased, showing sharply defined continuous staining (*). (D) At 8 days, there was both paracellular and punctate VE-cadherin immunoreactivity. (E-F) At 14-28 days sharply defined paracellular VE-cadherin immunoreactivity was present together with punctuate staining and resembled the VE-cadherin profile seen in control inferior colliculus tissue. Scale bar = 20 μm (refers A-F). Western blot analysis showed 3-chloropropanediol induced changes in VE-cadherin expression. (G) VE-cadherin expression showed 3 bands at 43 kDa (white bars), 126 kDa (black bars) and 184 kDa (hatched bars). At 2-4 days there was marked increased expression of 126 and 184 kDa bands with a slight change in the 43 kDa band. By 6-8 days there was a marked reduction in 126 kDa and 184 kDa band expression and were comparable to control levels. Protein quantification data was obtained by densitometry and was normalized using glyceraldehyde 3-phosphate dehydrogenase (GAPDH) as loading control. Values are expressed as relative optical density and are represented as mean ± s.e.m. *p<0.05, **p<0.01, ***p<0.001, compared to the control group. For each column n=4 rats.

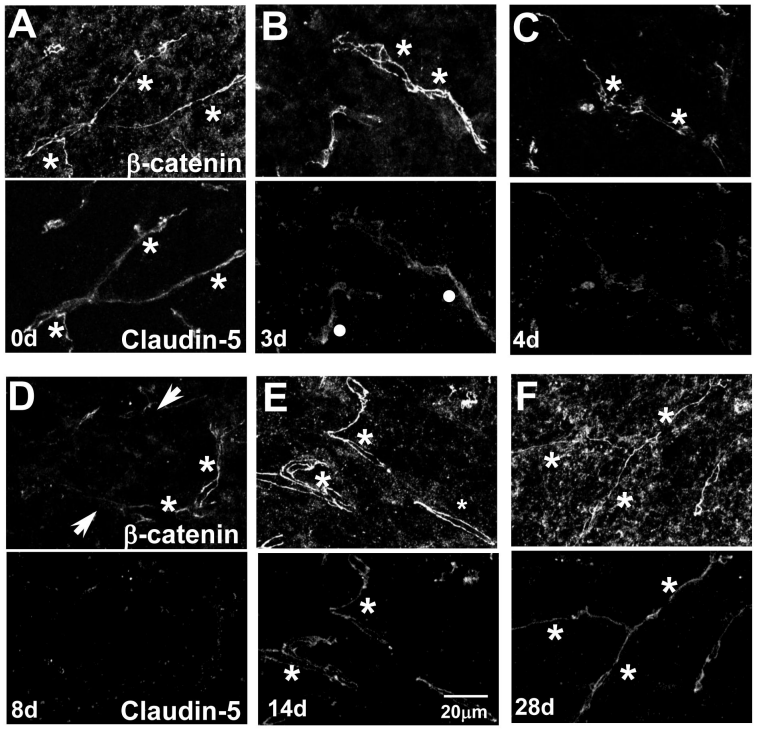

Figure 3.

Confocal micrographs showing the relationship between β-catenin and claudin-5 immunoreactivity following 3-chloropropanediol-induced changes in the inferior colliculus. Sections were double labeled for β-catenin and claudin-5 immunoreactivity. (A) In control tissue (0 days), β-catenin immunoreactivity mirrored that seen for claudin-5 and appeared as sharply defined paracellular expression (*). (B) At 3 days, many vessels showed sharply defined paracellular β-catenin immunoreactivity (*) while claudin-5 expression was greatly reduced and showed a largely diffuse immunoreactivity (dots). (C) At 4 days, paracellular β-catenin immunoreactivity (*) was maintained while claudin-5 expression was lost. (D) At 8 days, β-catenin immunoreactivity appeared as both paracellular (*) and punctuate (arrows) while claudin-5 showed faint diffuse immunoreactivity. (E) At 14 days, there was increased β-catenin immunoreactivity (*) and both paracellular (*) and diffuse claudin-5 expression. (F) At 28 days, immunoreactivity profile for both β-catenin and claudin-5 resembled that seen in control tissue. Scale bar = 20 μm (refers A-F). n=4 rats.

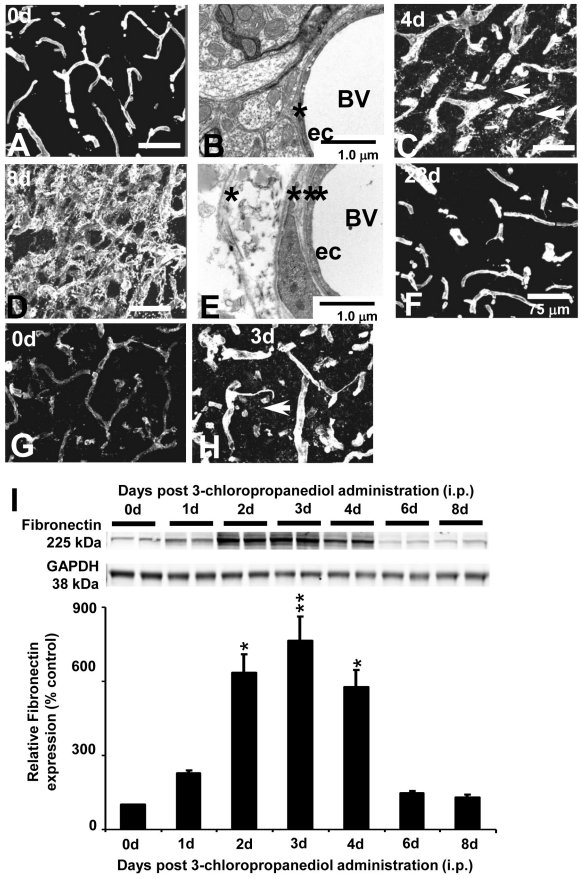

Figure 4.

Confocal micrographs of laminin and fibronectin immunoreactivity and electron micrographs of basement membrane in the inferior colliculus following 3-chloropropanediol (140 mg/kg i.p.) administration. (A) At 0 days, laminin immunoreactivity formed a smooth sheath around the underlying vascular endothelium. No laminin immunoreactivity was seen in the parenchyma. (B) At 0 days, electron micrograph showed vascular endothelial cell (ec) surrounded by fused basement membranes (*). (C) By 4 days, laminin remodeling was apparent. Laminin profiles were more irregular around the vascular endothelium (arrows). (D) At 8 days, extensive deposition of laminin immunoreactivity. Laminin profiles were highly irregular and laminin immunoreactivity was also seen in the parenchyma. (E) At 8 days, electron micrograph shows several layers of non-fused basement membranes (*****) and deposition of collagen/extracellular matrix components (◆) surrounding the vascular endothelial cell (ec), (F) By 28 days, laminin profiles resembled that seen in control tissue. (G) At 0 days, fibronectin immunoreactivity formed a smooth sheath around the underlying vascular endothelium. No fibronectin immunoreactivity was seen in the parenchyma. (H) By 3 days, fibronectin remodeling was apparent with irregular profiles around the vascular endothelium and immunoreactivity present in the parenchyma (arrows). Figures A,C,D,F,G;H scale bar = 75 µm. Figures B,E scale bar = 1.0 µm. (I) Western blot analysis showed 3-chloropropanediol induced changes in fibronectin expression. Fibronectin expression appeared as a 225 kDa band. At 2-4 days there was marked increased fibronectin expression. By 6-8 days, there was a marked reduction in fibronectin and were comparable to control levels. Protein quantification data was obtained by densitometry and was normalized using glyceraldehyde 3-phosphate dehydrogenase (GAPDH) as loading control. Values are expressed as relative optical density and are represented as mean ± s.e.m. *$p<0.05$, **$p<0.01$, compared to the saline control group. For each column n=4 rats.

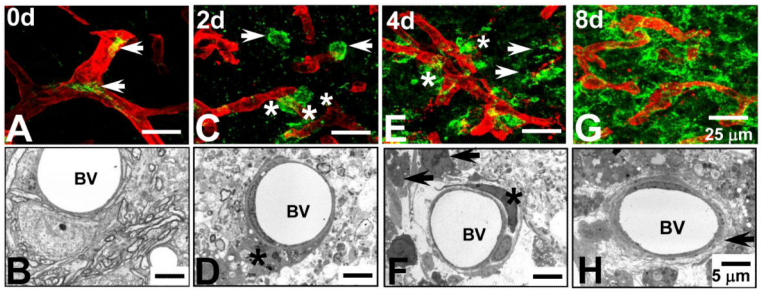

Figure 5.

Confocal and electron micrographs showing increased expression of CD169 immunoreactive macrophages (green) and leukocyte infiltration in the inferior colliculus following 3-chloropropanediol (140 mg/kg i.p.). (A-B) In control tissue, few CD169 immunoreactive macrophages were colocalised on the laminin immunoreactive (red) microvasculature. Electron micrograph shows a single fused basement membrane around a blood vessel (BV). No leukocytes were apparent. (C-D) At 2 days, increased numbers of CD169 immunoreactive macrophages were present in close association with laminin immunoreactive microvasculature. Electron micrograph shows a phagocytic leukocyte (*) with processes surrounding the vascular endothelial cell is present in the inferior colliculus. (E-F) At 4 days, further infiltration of CD169 immunoreactive macrophages was seen. Electron micrograph shows increased leukocyte infiltration around a blood vessel (*) and in the parenchyma (arrows). (G-H) At 8 days, massive macrophage infiltration had developed. Phagocytic leukocyte with extracellular matrix deposition (arrowed). Figures A,C,E,G scale bar = 20 µm, Figures B,D,F,H scale bar = 5 µm.